Synthesis, and Structural Characterization of 5,10,15,20-*tetrakis*-(2,6-dimethyl-4-fluorophenyl)porphyrinatoplatinum(II) for the Application of Oxygen Sensing

Zane S. Dash,[§] Raymond Q. Huang,[§] Ana N. Kimber,[§] Opeyemi T. Olubajo,[§] Mark Polk,[§] Oliver P. Rancu,[§] Lauren L. Zhang,[§] Jane Fu, Nejc Nagelj, Kristopher G. Reynolds, Shao-Liang Zheng and Dilek K. Dogutan*

Department of Chemistry and Chemical Biology, Harvard University, Cambridge, MA 02138, USA. *Correspondence e-mail: dkiper@fas.harvard.edu. [§]The authors contributed equally.

Abstract: The 5,10,15,20-*tetrakis*-(2,6-dimethyl-4-fluorophenyl)porphyrinatoplatinum(II)porphyrin [Pt(II)TFP] has been synthesized and structurally characterized by single crystal X-ray crystallography. The Pt porphyrin exhibits a long-lived phosphorescent excited state (τ = 66 μs), which has been characterized by transient absorption and emission spectroscopy. The phosphorescence is extremely sensitive to oxygen, as reflected by a quenching rate constant of 5.0×10^8 M^{-1} s^{-1} and measured by Stern-Volmer quenching analysis.

Keywords: crystal structure, platinum porphyrin, oxygen sensing, time resolved absorption spectroscopy, time resolved emission spectroscopy.

1. Introduction

Porphyrins comprise four pyrrole subunits connected by methine bridges at their α carbon atoms, leading to extensive π-conjugation that engenders intense light absorption and emission properties (Gouterman & Dolpin 1978; Ghosh, 2000). With their distinct photophysical and photochemical properties, porphyrins have emerged as versatile molecules for a variety of chemical, biomedical, environmental and sensing applications (Paolesse *et al*., 2017). The porphyrin macrocycle can strongly bind metal ions within their central cavity; the identity of the bound metal can significantly influence the electronic structure of the macrocycle. Owing to spin-orbit coupling, the residency of Pt in the macrocycle cavity gives rise to an especially intense and long-lived phosphorescence, engendering their utility in energy conversion processes (Akamine *et al.*, 2020; Cao *et al.*, 2021; Gao *et al.*, 2022; Gu *et al.*, 2020; Morifuji *et al.*, 2019) and bioimaging (Nagai *et al.*, 2015; Odai *et al.*, 2019; Zhang *et al.*, 2022). Optical oxygen sensors based on Pt porphyrins are attractive due to their reversibility, lack of analyte consumption, non-invasiveness, precision, and versatility (Wang & Wolfbeis, 2014). An especially important biomedical application of Pt porphyrins arises from the extreme sensitivity of their phosphorescent excited states to quenching by oxygen (Buchler *et al.*, 1995, Jana *et al.*, 2016; Papkovsky & O'Riordan, 2005). The generated singlet oxygen from this efficient quenching reaction is cytotoxic to tumor cells, thus engendering the utility of Pt porphyrins in photodynamic therapy (PDT) (Couto *et al*., 2020).

Given the wide-range applications of Pt porphyrins, we sought to expand the repertoire of known Pt porphyrins with the use of the 5,10,15,20-*tetrakis*-(2,6-dimethyl-4-fluoro-phenyl)porphyrin (TFP) platform. The 4-fluoro-2,6-dimethylphenyl substituents on the four *meso* positions of the macrocycle makes this motif a particularly useful synthon with regards to both synthetic versatility and the utility of the fluoro group as a handle for NMR characterization (Chou *et al.*, 2022; Brown *et al.*, 2023). We now report the synthesis and full characterization of Pt(II)TFP including its crystal structure, and assess its oxygen quenching properties via transient absorption and emission spectroscopy.

2. Experimental

2.1. Synthesis, purification and crystallization

$PtCl_2$ was purchased from Sigma-Aldrich and used as received. 5,10,15,20-*tetrakis*(4-fluoro-2,6-dimethylphenyl)-porphyrin (TFP) was synthesized by following previously reported procedures (Chou *et al.*, 2022; Brown *et al.*, 2023). Tetrabutylammonium hexafluorophosphate ($TBAPF_6$) was obtained from Sigma-Aldrich, recrystallized from EtOH, dried for two days under vacuum on a Schlenk line without heat, and stored in a nitrogen-filled glove box. Electrolyte solution was stored over activated 3 Å molecular sieves before use. ^1H and ^{19}F NMR spectra were recorded at the Harvard University Department of Chemistry and Chemical Biology Laukien-Purcell Instrumentation Center on a JEOL ECZ400S spectrometer operating at 400 MHz. Absorption spectra were taken with a 1.0 cm quartz cuvette on a Varian Cary5000 UV−vis-NMR spectrophotometer (Figure 2, Top). Steady-state emission spectra were measured on a fluorimeter (Photon Technology International, PTI model QM4) coupled to a 150 W Xe arc lamp as an excitation light source. Mass spectrometry was performed at the Harvard Center for Mass Spectrometry. Crystallography data was collected at the Harvard University Department of Chemistry and Chemical Biology X-Ray Facility. Steady-state emission spectra (Figure 2 bottom) were measured on a fluorimeter (Photon Technology International, PTI model QM4) coupled to a 150 W Xe arc lamp as an excitation light source. Steady

state emission spectra were collected in anhydrous toluene in 1 cm four-sided quartz cuvettes with 400 nm excitation corresponding to the Soret band absorption. The cuvettes were sealed with rubber septa and purged for 30 min with nitrogen and a gas mixture containing 2% oxygen, forced air, or 100% oxygen and vented to equilibrate the pressure to atmospheric pressure.

The freebase TFP porphyrin was metalated by following reported procedures (Wu, 2011) with a slight modification. $PtCl_2$ (93.33 mg, 0.35 mmol) was added in benzonitrile (84 mL) and heated with a heat gun until $PtCl_2$ was completely dissolved. TFP (30 mg, 0.038 mmol) was added into the $PtCl_2$ solution in benzonitrile and the resulting mixture was heated at reflux for 48 h. The progress of the metalation reaction was monitored with thin layer chromatography. Upon consumption of all TFP, the mixture was cooled to room temperature and benzonitrile was removed under vacuo distillation. The resulting crude porphyrin was subsequently redissolved in CH_2Cl_2 (10 mL), treated with triethylamine (TEA, 1 mL), washed with water and brine, and dried over Na_2SO_4. The solvent was removed in vacuo, and the residue was subsequently redissolved in CH_2Cl_2 (~10 mL). The CH_2Cl_2 solution was introduced onto a Biotage automated flash silica column chromatography instrument and eluted with a gradient of 0–30% Hexanes/CH_2Cl_2. The title compound was isolated as an orange-red powder (25.9 mg, 69.5 % isolated yield). ^{1}H NMR (400 MHz, CD_2Cl_2) δ (ppm): 8.55 (s, 8H), 7.18 (d, J = 8 Hz, 8H), 1.88 (s, 24H). ^{19}F NMR (379 MHz, CD_2Cl_2) δ(ppm): − 116.02 (triplet due to ^{1}H–^{19}F J = 9.48 Hz, 4F). HR-MS [$(M+H)^+$, M = $C_{52}H_{40}PtF_4N_4$]: m/z calcd (obsd), 992.2913 (992.2900). MALDI-TOF 991.985. λ_{abs} (toluene) 399, 509, 539 nm.

Dark red-orange crystals of Pt(II)TFP were grown through vapor-diffusion of pentanes (anti-solvent) onto CH_2Cl_2 (good solvent) at –36 °C in nitrogen filled glovebox. After a one-week waiting period, shiny orange-red crystals were obtained.

2.2. Refinement

Table 1 contains crystal data, data collection, and structure refinement details. A single red-orange plate-shape crystal (0.180 mm × 0.090 mm × 0.080 mm) was chosen for single-crystal X-ray diffraction using a Bruker D8 goniometer equipped with a Photon III C-14 area detector. Data were collected as a series of φ and/or ω scans. The crystal is merohedrol twin, but the structure has been refined by using reflections in hkl5 format that is created by Cell_Now/Twinabs. Data integration down to 0.84 Å resolution was carried out using SAINT V8.40A with reflection spot size optimization. Absorption corrections were made with the program TWINABS. Space-group assignments were determined by examination of systematic absences, E-statistics, and successive refinement of the structures. The structure was solved by the intrinsic phasing method and refined by least-squares methods also using SHELXT2019, SHELXL2019/1, and Bruker SHELXTL (Sheldrick, 2014, 2015a, 2015b, Krause *et al.,* 2015) with the OLEX2 (Dolomanov *et al.*, 2009) interface, Bruker AXS APEX3, Bruker AXS (Madison & Wisconsin, 2019)

Table 1
Experimental structural details.

Crystal data	
Chemical formula	$C_{52}H_{40}F_4N_4Pt$
MW	991.97
Crystal system	Tetragonal
Space group	*I*4/*m*
Temperature (K)	100
a (Å)	17.1883(13)
b (Å)	17.1883(13)
c (Å)	9.1123(9)
α (°)	90
β (°)	90
γ (°)	90
V (Å^3)	2692.1(5)
Z	2
Radiation type	Mo Kα
μ (mm^{-1})	2.65
Crystal size (mm)	0.18 × 0.09 × 0.08
Data Collection	
Diffractometer	Bruker D8
Absorption correction	Multi-scan
T_{min}, T_{max}	0.391, 0.490
No. of meas. independent and obsd [I > 2σ(I)] reflns	1785, 1785, 1773
R_{int}	0.062
$(\sin\theta/\lambda)_{max}$ (Å^{-1})	0.596
Refinement	
R[F^2 > 2σ (F^2)], wR(F^2), S	0.033, 0.072, 1.05
No. of reflns	1785
No. of parameters	85
H-atom treatment	H-atom parameters constrained
$\Delta\rho_{max}$, $\Delta\rho_{min}$ (e Å^{-3})	1.22, -0.73

Computer programs: SAINT 8.40A (Bruker-AXS, 2019), SHELXT2019 (Sheldrick, 2015), SHELXL2019/1 (Sheldrick, 2015), Bruker SHELXTL (Sheldrick, 2015).

(Dolomanov, *et al.*, 2009). The program PLATON (Spek, 2002) was employed to confirm the absence of higher symmetry space groups. All non-H atoms were located in difference-Fourier maps, and then refined anisotropically. Hydrogen atoms on C atoms were placed at idealized positions and refined using a riding model. The isotropic displacement parameters of all hydrogen atoms were fixed to 1.2 times the atoms they are linked to (1.5 times for methyl groups). The severely disorder solvent molecules with total electrons 172, which were found in a total 896 Å^3 solvent accessible volume in per unit cell (2692 Å^3), could not be located in the Fourier map and have been squeezed out by using PLATON/SQUEEZE (Spek, 2002, 2015a, 2015b).

The crystal structure and the packing diagrams of Pt(II)TFP are presented in Figure 1. The molecule is packed along the 4_1 screw axis when viewing along crystallographic c axis. Additionally, there are large cavities viewed along c, and the solvent accessible volume, calculated by using Platon (Spek, 2002, 2015a, 2015b) is up to 896 Å^3 (Spek, 2002, 2015) in per unit cell (2692 Å^3), and the severely disordered solvents that couldn't be located from the difference map have been squeezed out.

3. Results and discussion

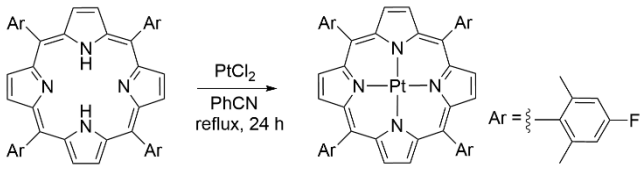

Scheme 1. Synthesis of Pt(II)TFP.

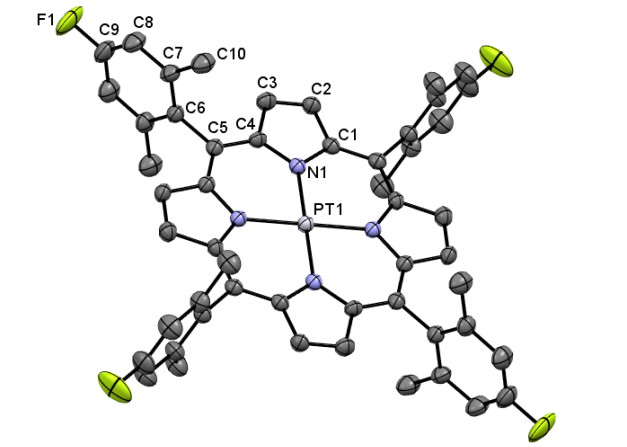

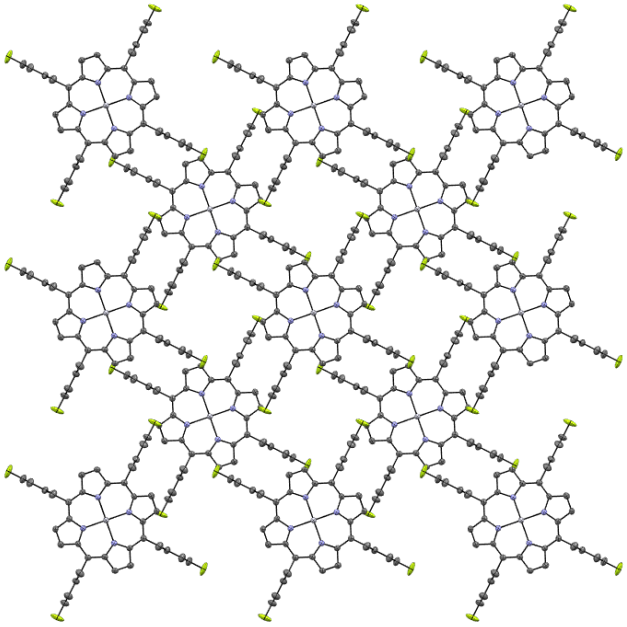

Figure 1. Top: Ellipsoid plot of the title compound, with the asymmetric unit atom- numbering scheme. Displacement ellipsoids are drawn at the 50% probability level. Hydrogen atoms are omitted for clarity. Bottom: Crystal packing of the Pt(II)TFP along crystallographic c axis showing the cavity between Pt(II)TFP. Color scheme: C (gray), N (light purple), F (yellow-green), Pt (white). The packing along the a-axis and the b-axis is provided in Fig. S8.

Characterization and Structural Chemistry. The preparative route for the metalation of TFP with Pt(II) and the chemical structure of Pt(II)TFP are shown in Scheme 1. Metalation of TFP with $PtCl_2$ was achieved via deprotonation of the internal N-H pyrrolic protons in the absence of externally added base. The ^{1}H NMR spectrum of Pt(II)TFP confirms disappearance of the inside pyrrolic NH resonances while showing the typical resonances for fully symmetric metalated A4 porphyrin structure. In the ^{19}F NMR spectrum,

Table 2

Selected geometric parameters (Å,º) for Pt(II)TFP.

Bond distances (Å)		
Pt–Ni	Pt1–Ni1^{i}	2.014(4)
Pt–Ni	Pt1–Ni1^{ii}	2.014(4)
Pt–Ni	Pt1–Ni1^{iii}	2.014(4)
Pt–Ni	Pt1–Ni1	2.014(4)
Selected bond angles (º)		
Ni–Pt–Ni	N1^{i}–Pt1–N1^{iii}	90
Ni–Pt–Ni	N^{ii}–Pt1–Ni^{iii}	90
Ni–Pt–Ni	N1^{i}–Pt1–N1	89.999(1)
Ni–Pt–Ni	N1^{ii}–Pt1–N1	90
Selected torsional angles (º)		
C–C–C	C7^{iv}–C6–C5	119.7(2)
C–C–C	C7–C6–C5	119.7(2)

Symmetry codes: (i) $y, -x + 1, -z + 1$; (ii) $-y + 1, x, z$; (iii) $-x + 1, -y + 1, -z + 1$; (iv) $x, y, -z + 1$.

the triplet at –116.02 ppm arises from coupling the two chemically equivalent protons located on the 3 and 5 positions of the 4-fluoro,2,6-dimethylphenyl group. ^{1}H (Figs. S1–S3) and ^{19}F (Figs. S4 and S5) NMR spectra are provided in the Supporting Information. The H-F J-coupling constant for the ^{1}H NMR was confirmed as 8 Hz and the ^{1}H–^{19}F coupling constant was observed to be 9.48 Hz. In addition to NMR, high-resolution (Fig. S6) and MALDI-TOF (Fig. S7) mass spectrometry are consistent with a Pt(II)TFP compound formulation.

Figure 1 shows the structure of Pt(II)TFP as deduced from single-crystal X-ray diffraction analysis. The compound crystallizes in the *I*4/m space group. Pertinent bond metrics for Pt(II)TFP are presented in Tables 2. Complete tables of the structural metrics of the porphyrin are listed in Tables S1 and S2 of the supporting information. The Pt(II)TFP structure shown possesses a perfect square planar geometry where Pt(II) occupies the inversion center, as has also been observed for its Pd(II) congener (Crisp *et al.*, 2022). The asymmetric units contain 1/8 of the molecules which upon inversion about the platinum yields the complete molecular structure. The four central platinum pyrrolic nitrogen bonds were observed as two identical sets showing the same distance as 2.014(4) Å which is consistent with the previously reported square planar fully symmetric Pt(II) porphyrins in the D_{4h} point group (Che *et al.*, 2003; Masamichi *et al.*, 2003; Poornenth *et al.*, 2017; Senge & Richter 2011).

Spectral Properties of Pt(II)TFP. The UV-vis absorption spectrum of Pt(II)TFP is shown in Figure 2. In accordance with the Gouterman four orbital model (Gouterman, 1959, 1961, Gouterman *et al.*,1963), the absorption profile is dominated by the Soret band at 399 nm (261,000 M^{-1} cm^{-1}) with two Q bands at 508 nm (21,900 M^{-1} cm^{-1}) and 539 nm (8,380 M^{-1} cm^{-1}). The effective D_{4h} symmetry of Pt(II)TFP leads to fewer Q bands as compared to those observed of the freebase porphyrins, where TFP (Chou *et al.*, 2022) has D_{2h} symmetry. Additionally, there is a significant hypsochromic shift of the Soret band of Pt(II)TFP relative to TFP (λ_{max} (Soret) = 430 nm) as is characteristic for porphyrins with metals with d-electron counts > 6. The hypsochromic effect of d^n (n > 6) metalloporphyrins has traditionally been

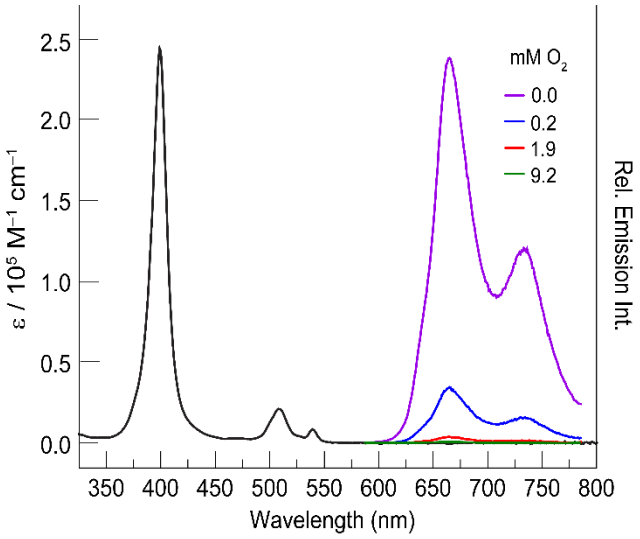

Figure 2. Absorption and emission spectrum of Pt(II)TFP recorded in dry toluene at room temperature. The quenching of the steady state emission spectrum is shown with increasing concentrations of O_2. A Stern-Volmer fit of the data according to Eq. (1) yields an oxygen quenching rate constant of 5.0×10^8 M^{-1} s^{-1}.

ascribed to an increase in the HOMO−LUMO gap arising from the destabilization of the porphyrin e_g LUMOs due to metal(dπ)−porphyrin(LUMO) backbonding interactions. However, high level DFT and time-dependent density functional theory (TDDFT) computations have revealed that the e_g orbitals remain relatively constant in energy and the increased HOMO-LUMO gap results from the stabilization of the a_{2u} HOMOs for Pd(II) and Pt(II) porphyrins (Ghosh & Conradie 2021).

Platinum(II) residing in the porphyrin ring is considered as a redox inactive metal due to the high lying $d_{x^2-y^2}$ orbital residing within the tetragonal ligand field of the porphyrin macrocycle (Kadish *et al*., 1975, 2000). The cyclic voltammogram (CV) of Pt(II)TFP in a nitrogen filled glovebox using 0.1 M $TBAF_6P$ in CH_2Cl_2 as the electrolyte solution is shown in Fig S9. One-electron, reversible oxidation and reduction waves are observed at 0.78 V and –1.85 V, respectively. Previous studies of Pt(II) tetraphenylporphyrin have ascribed these redox events to be associated with one-electron ligand-based processes of the macrocycle (Ou *et al*., 2010). Consistent with this assignment, the reduction of TFP (freebase porphyrin) occurs at –1.80 V, (Chou *et al*., 2022) which is similar to the Pt(II)TFP reduction wave.

Oxygen Quenching of Electronically Excited Pt(II)TFP. To evaluate the oxygen sensing properties of Pt(II)TFP, we quantified the emission intensity in the presence of varying concentration of oxygen. An emission lifetime of 66 µs is measured for Pt(II)TFP under a nitrogen atmosphere; this lifetime is within the 50-100 µs lifetime range observed for various Pt porphyrins (Baggaley *et al*., 2012). After bubbling 100% oxygen gas, the phosphorescence intensity was almost completely quenched.. The quenching kinetics from Stern-Volmer analysis,

$$\frac{I_0}{I} = 1 + k_q \tau_0 [O_2] \quad (1)$$

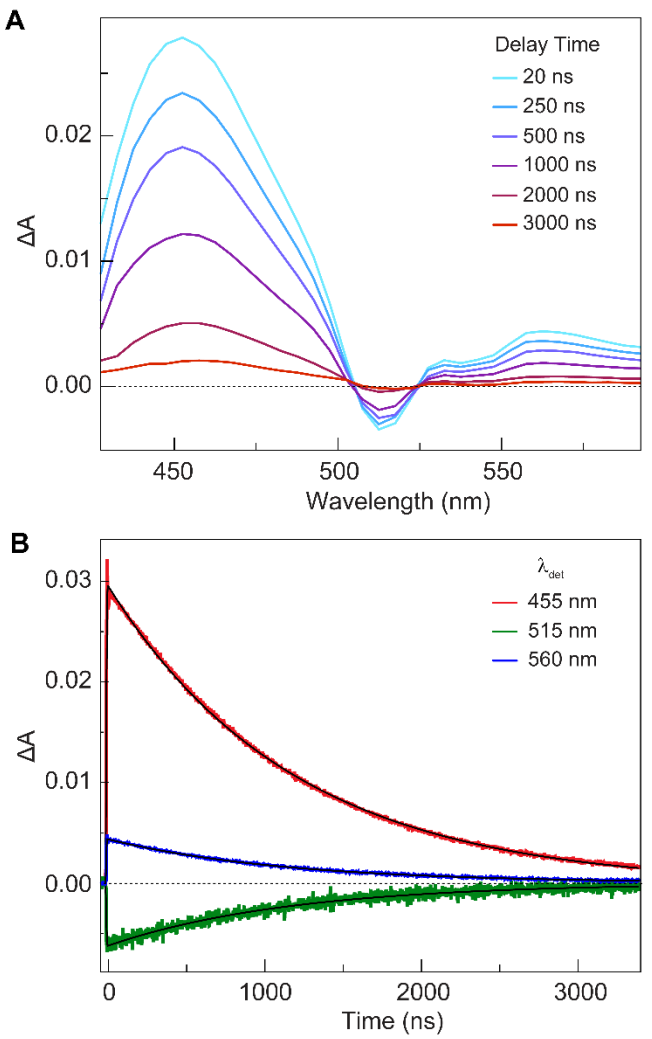

Figure 3. (**A**) Pt(II)TFP transient absorption spectrum of Pt(II) TFP in toluene in the presence of air recorded at the indicated times after the laser pulse. (**B**) Time-resolved kinetics for the decay of the Pt(II) TFP in toluene in the presence of air at the maxima of the absorption and bleaching signals in the TA spectrum. The decay curves fit a mono-exponential with a lifetime of 1.16 ± 0.03 µs.

where I_o and I are the emission intensity in the absence and presence of oxygen, respectively, and τ_0 is the excited state lifetime for Pt(II)TFP under nitrogen. The concentration of dissolved oxygen (0.19 to 9.2 mM) in anhydrous toluene was determined using a Henry's law constant of 104.5 MPa at 298.34 K (Fischer & Wilken 2001). A Stern-Volmer plot yields a quenching rate constant of 5.0×10^8 M^{-1} s^{-1}.

The quenching observed in steady-state emission measurements is recapitulated in measurements of the time-resolved absorption spectrum of the phosphorescent excited state. The TA spectrum and associated decay kinetics were collected on the EnVision (Magnitude Instruments) spectrometer. Briefly, samples where photoexcited at 355 nm with an internal nanosecond pulsed laser with a pulse width of 5 ns at 6 kHz and a per pulse energy of 80 µJ. Excited state absorptions were probed with a Xe-arc lamp. TA spectra were reconstructed from individual kinetic traces. The TA spectrum shows two pronounced maxima for the phosphorescent excited state at 455 and 560 nm, accompanied by a bleaching signal of the ground state Q-band at 515 nm. Under air, the time resolved kinetics

measured at these maxima are in good agreement, yielding a consistent lifetime of 1.16 (±0.03) μs. This lifetime is concordant with the measured emission lifetime of 1.3 μs for air saturated solutions of Pt(II)TFP.

4. Conclusion

Pt(II)TFP has been synthesized and structurally characterized by single X-ray crystallography. Pt(II)TFP exhibits a long-lived phosphorescent excited state (τ_o = 66 μs), which has been characterized by transient absorption and emission spectra. The triplet excited state of Pt(II)TFP is efficiently quenched by oxygen; a quenching rate constant of 5.0×10^8 M^{-1} s^{-1} is measured by Stern-Volmer analysis. Such a high rate constant is consistent with the extreme sensitivity of Pd(II) and Pt(II) porphyrins to oxygen, underpinning the importance of these compounds as O_2 sensors and triplet sensitizers of singlet oxygen.

Acknowledgements

This research was conducted as a portion of the CHEM 145 Experimental Inorganic Chemistry Course at Harvard University. DKD acknowledges Harvard University Chemistry and Chemical Biology Department for their kind support. We thank Professor Daniel G. Nocera for the helpful discussions and contributions to the preparation of this manuscript. We thank the support to the X-ray facility from the Major Research Instrumentation (MRI) Program of the National Science Foundation (NSF) under Award Numbers 2216066.

References

Akamine, K., Morita, K., Sakai, K. & Ozawa, H.(2020) *ACS Appl. Energy Mater.* **3**, 4860−4866.

Baggaley, E., Weinstein, J. A. & Williams, J. A. G. (2012). *Coord. Chem. Rev.* **256**. 1762–1785

Brown, C., Campbell, B. M., Chen, T., Darkwa, R. K., Kim, G., Kranchalk, D. J., Lamport, H., Le, C. M-D., Lu, J., McKnight, G. N., Nagelj, N., Seshadri, N. V., Reynolds, K. G., Zheng, S-L. & Dogutan, D. K. (2023). *J. Porphyrins Phthalocyanines* 27, 1–9.

Buchler, J. W., Dreher, C. & Kunzel, F. M. (1995). *Struct. Bonding*. **84**, 1−69,

Madison, Wisconsin, Bruker AXS APEX3, Bruker AXS, 2019.

Cao, L., Li, J., Zhu, Z.-Q., Huang, L. & Li, J. (2021). *ACS Appl. Mater. Interfac.* **13**, 60261–60268.

Che, C.-M., Hou, Y.-J., Chan, M. C. W., Guo, J., Liu, Y. & Wang, Y. (2003). *J. Mater. Chem.* **6**, 1362–1366.

Chou, P., Kim, L., Marzouk, S. M., Sun, R., Hartnett, A. C., Dogutan, D. K., Zheng, S. H. & Nocera, D. G. (2022) *ACS Omega*, **7**, 8988–8994.

Couto, G. K., Pacheco, B. S., Borba, V. M., Rodrigues Junior, J. C., Oliveira, T. L., Segatto, N. V., Seixas, F. K., Acunha, T. V., Iglesias, B. A. & Collares, T. (2020). *J. Photochem. Photobiol. B* **202**, 111725.

Crisp, W., Fagan-Avery S. A., Campbell, B. M., Morphet, D. R., Reynolds, K. G., Kudisch, B., Gonzalez, M. I. & Zheng, S-H. (2022) *Inorg. Chem. Commun.* **146**, 109999.

Dolomanov, O. V., Bourhis, L. J., Gildea, R. J., Howard, J. A. K. & Puschmann H. (2009). *J. Appl. Cryst*. **42**, 339–341.

Fischer, K. & Wilken, M. (2001). *J. Chem. Thermodyn*. **33**,1285−1308.

Gao, Y., Piradi, V., Zhu, X. & So, S. K. (2022). *ACS Appl. Energy Mater.* **5**, 4916–4925.

Gouterman, M. J. (1959). *J. Chem. Phys*. **30**,1139–1161.

Gouterman, M. J. (1961). *J. Mol. Spectrosc*. **6**, 138–163.

Gouterman, M. J., Snyder, L.C. & G.H. Wagniere. (1963). *J. Mol. Spectrosc*. **11**, 108–127.

The Porphyrins (1978) edited by Dolphin, D., Gouterman, M. (1978) (ed), vol. III, Part A, *Physical* Chemistry, Academic Press: New York.

The Porphyrin Handbook (2000). edited by Ghosh, A. Vol. 7, Ch. 47, *Theoretical and Physical Characterization*, Kadish, K. M., Smith K. M. & Guilard, R. (eds), Academic Press: San Diego, CA.

Ghosh, A. & Conradie, J. (2021) *J. Phys. Chem.* **125**, 9962−9968.

Gu, W., Nishikubo, R. & Saeki, A. (2020) J. Phys. Chem. C **124**, 14439−14445.

Jana, A., McKenzie, L., Wragg, A. B., Ishida, M., Hill, J. P., Weinstein, J.A., Baggaley, E. & Ward, M. D. (2016). *Chem. Eur. J.* **22**, 4164–4174.

The Porphyrin Handbook. (2000). edited by K. M. Kadish, K. M. Smith, R. Guilard. K. M. Kadish, E. Van Caemelbecke, G. Royal, Academic Press, New York. Vol. 8, Ch. 55, pp 1–114.

Porphyrins and Metalloporphyrins. (1975). edited by K. M. Smith. J.-H. Fuhrhop, American Elsevier Publishing Co. Inc., New York. Vol. Ch. 14, pp 593–624.

Krause, L., Herbst-Irmer, R., Sheldrick, G. M., Stalke, D. (2015) *J. Appl. Crystallogr*. **48**, 3-10.

Masamichi, U., Ken-ichi, S., Hitoshi, M., Tomohiko, I. & Masahiro, Y. (2003). *Bull. Chem. Soc. Jpn.* **76**, 2123–2127.

Morifuji, T., Takekuma, Y. & Nagata, M. (2019). *ACS Omega.* **4**, 11271–11275.

Nagai, A., Miller, J. B., Kos, P., Elkassih, S., Xiong, H. & Siegwart, D. J. (2015). *ACS Biomater. Sci. Eng.* **1**, 1206–1210.

Odai, S., Ito, H. & Kamachi, T. (2019). *J. Clin. Biochem. Nutr.* **65**, 178–184.

Paolesse, R., Nardis, S., Monti, D., Stefanelli, M., Di Natale, C. (2017) *Chem Rev.* **117**, 2517–2583.

Poornenth, P., Maurya, Y. K., Omagari, T., Hirosawa, R., Ishida, M., Mori, S., Yasutake, Y., Fukatsu, S., Mack, J., Nyokong, T. & Furuta, H. (2017). *Inorg. Chem.* **56**, 12572–12580.

Papkovsky, D. B. & O'Riordan, T. C. (2005). *J. Fluoresc*. **15**, 569−584.

Ou, Z., Chen, P. & Kadish, K. M. (2010). *Dalton. Trans.* **39**, 11272–11276.

Senge, M. O. & Richter, J. (2011). *Acta Cryst.* E**67**, m1077.

Sheldrick, G. M. (2014) SHELXL, University of Göttingen, Germany.

Sheldrick, G. M. (2015a) *Acta Cryst.* **A71**, 3–8.

Sheldrick, G. M. (2015b) *Acta Cryst.* **C71**, 3–8.

Spek, A. L. (2002) *J. Appl. Cryst.* **36**, 7–13.

Spek, A. L. (2015b). *Acta Cryst.***C71**. 9-18.

Wang, X.-D. & Wolfbeis, O. (2014). *Chem. Soc. Rev.* **43**, 3666–3761.

Wu, W., Wu, W., Ji, S., Guo, H., Wang, X., & Zhao, J. (2011). *Dyes Pigments* **89**, 199–211.

Zhang, W., Chen, S., Sun, P., Ye, S., Fan, Q., Song, J., Zeng, P., Qu, J. & Wong, W.-Y. (2022). *Adv. Healthcare Mater.* **11**, 2200467.